Molecular Structure of a Supported VO_4 Cluster and Its Interfacial Geometry as a Function of the SiO_2, Nb_2O_5, and ZrO_2 Support

Daphne E. Keller, Diek C. Koningsberger, and Bert M. Weckhuysen*

Inorganic Chemistry and Catalysis, Department of Chemistry, Utrecht University, P.O. Box 80083, 3508 TB Utrecht, The Netherlands

Received: February 4, 2006; In Final Form: April 18, 2006

The influence of the support oxide on the molecular structure of a VO_4 cluster and its interfacial geometry has been determined for SiO_2, Nb_2O_5, and ZrO_2 as supports. Raman, IR, UV−vis−NIR diffuse reflectance, electron spin resonance, and extended X-ray absorption fine structure (EXAFS) spectroscopies were used to characterize the supported vanadium oxide clusters after dehydration. It has been found that for all supports under investigation the vanadium ion is tetrahedral coordinated and consists of one V═O and three V−O bonds. For a VO_4/SiO_2 catalyst it has been established that only one O neighbor is shared with the SiO_2 support via a $V-O_b-Si_{support}$ bond with an angle of ∼101° (±0.5°) and a V···Si distance of 2.61 Å. The absence of a second vanadium atom in the vicinity of the vanadium oxide cluster further subverts the classical assignment of the 920 cm^{-1} Raman band to a V−O−V related vibration. The EXAFS results combined with structural modeling using Cerius[2] software lead to structural constraints, which imply a similar $V-O_b-M_{support}$ interaction for Nb_2O_5 and ZrO_2 as well. The $V-O_b$ and the $V\cdots M_{support}$ distances depend on the geometry of each support surface. The results show that the classical model with three $V-O_b-M_{support}$ bonds could not be experimentally observed with EXAFS under the applied measuring conditions. Additional experiments with IR and Raman spectroscopy under experimental conditions mimicking those of the EXAFS measurements reveal the presence of V−OH groups, giving further support for the presence of a $O═V(OH)_2-O_b-M$ moiety at the support surface.

1. Introduction

The catalytic properties of transition metal oxide catalysts are determined by several parameters, e.g., metal oxide loading, pretreatment conditions, molecular structure, electronic structure, and support material.[1−6] Although many researchers have studied the activity of metal oxide catalysts, it is still unclear which of the parameters mentioned above are truly responsible for the catalytic performance and which mechanism determines the catalytic operation.

It has already been shown that the catalytic activity in various oxidation reactions over transition metal oxide catalysts changes with the support material.[1,3,7] Although the nature of the support effect is fairly well described for metal particles,[8−10] the origin of the metal oxide support effect, however, is not yet well understood.

In general, the VO_4 monomeric species in dehydrated supported vanadium oxide catalysts has been envisaged as a distorted tetrahedral structure with one V═O bond and three $V-O_b-M_{support}$ bonds (Figure 1a).[11−15] This classical model is characterized by a vibration at ∼1020−1040 cm^{-1}, as measured with Raman spectroscopy.[16] The exact frequency depends on the support material. By comparison with reference compounds ($VOCl_3$, $VOBr_3$, and VOF_3) this band has been assigned to the V═O stretch vibrational mode for a short V═O bond.[16] ^{18}O labeling experiments, in conjunction with Raman spectroscopy, confirmed the mono-oxo nature of the VO_4 unit.[17,18] With Raman spectroscopy vibration modes due to the $V-O-M_{support}$ bond, which are believed to be active in catalysis, could not be observed. Other techniques have delivered little additional support for the existence of the classical model so far.[19−21]

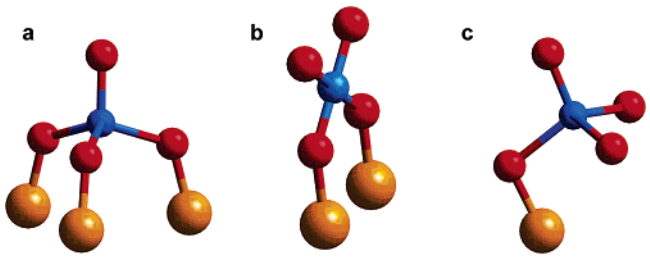

Figure 1. (A) Classical model, with three bonds to the support and one V═O bond. (B) Model with two bonds to the support, one V═O bond, and one V−O bond. (C) Umbrella model with one bond to the support ($V-O_b-M_{support}$), one V═O bond, and two V−O bonds.

Although the classical VO_4 model is the most widely accepted in the literature, one should also consider the possibility of one or two $V-O-M_{support}$ bonds instead of three (Figures 1b and 1c).[22−26] A recent study demonstrated with results obtained from extended X-ray absorption fine structure in combination with a structural model that for alumina-supported vanadium oxide species only one $V-O_b-M_{support}$ bond can be formed after dehydration.[27] The molecular structure of the interface between the support oxide material and the VO_4 cluster was determined. These results implied that the classical model with three $V-O-M_{support}$ bonds is less likely or at least not the exclusive structure at the catalyst surface. In this umbrella type model the vanadium has one V═O bond, two V−O bonds, and one $V-O_b-M_{support}$ bond, as is depicted in Figure 1c.[22,27] The consequence of the

* Author to whom correspondence should be addressed. E-mail: b.m.weckhuysen@chem.uu.nl.

10.1021/jp060749h CCC: $33.50 © 2006 American Chemical Society
Published on Web 07/01/2006

TABLE 1: Catalyst Codes and Some Physicochemical Data for All Vanadium Oxide Catalysts Discussed in This Paper

sample name	sample	loading (VO_x/nm^2)	% monolayer[a] monomer	% monolayer[a] polymer	S_{BET} (m^2/g)	V_{pore} (mL/g)	$I_{pre\text{-}edge}$	$E_{edge} - E_{pre\text{-}edge}$ (eV)	Raman shift (cm^{-1})	UV−vis DRS E (eV)
1V−Al	1 wt % V_2O_5/Al_2O_3	0.430	18.7	5.73	165	0.35	0.66	12.62	1024	3.19
1V−Nb	1 wt % V_2O_5/Nb_2O_5	0.399	17.3	5.32	188	0.18	0.61	13.62	1036	3.49
1V−Si	1 wt % V_2O_5/SiO_2	0.118	5.13	1.57	594	0.71	0.64	13.27	1041	3.34
1V−Zr	1 wt % V_2O_5/ZrO_2	0.743	32.3	9.91	100	0.23	0.51	12.83	1020	3.46

[a] The values for the monomeric (2.3 VO_x/nm^2) and polymeric (7.5 VO_x/nm^2) monolayer coverages are taken from Khodakov et al.[7]

umbrella model is that the support influence on the catalytic performance of vanadium as mentioned above acts via the $V-O_b-M_{support}$ bond. To further understand the origin of the support effect on the catalytic activity of the supported vanadium oxide catalyst, detailed knowledge on the vanadium oxide structure and the way the cluster is anchored to the surface is required for other supports as well. The mechanism of the support effect, either geometric or electronic, can only then be determined.

In the present paper we determine the influence of the support oxide on the molecular structure of a VO_4 cluster and its interfacial geometry. For this purpose, a series of low loaded (1 wt %) vanadium oxide catalysts has been prepared on several oxidic supports (Nb_2O_5, SiO_2, and ZrO_2). These catalysts were characterized with Raman and infrared (IR) spectroscopies, ultraviolet−visible−near-infrared diffuse reflectance spectroscopy (UV−vis−NIR DRS), and electron spin resonance (ESR) and extended X-ray absorption fine structure (EXAFS) spectroscopies after dehydration. At dehydrated conditions and low loading—below the monomeric monolayer (2.3 VO_x/nm^2) as defined by Khodakov[7]—the vanadium oxide species on the surface will be present only as a monomeric VO_4 cluster with one V═O bond.[17,18] EXAFS data analysis showed that for all supports the VO_4 cluster is attached to the surface with only one $V-O_b-M_{support}$ bond under the applied measurement conditions. Both the $V-O_b$ bond distance and the $V\cdots M_{support}$ distance depend on the structure of the support surface. The results will be compared with previously reported data on alumina-supported 1 wt % vanadium oxide catalyst. Additional experiments with IR and Raman spectroscopy measured under conditions similar to those applied for the EXAFS experiments show the presence of V−OH groups, pointing toward the presence of a $O{=}V(OH)_2-O_b-M_{support}$ surface species.

2. Experimental Section

2.1. Catalyst Preparation. A series of supported vanadium oxide catalysts with 1 wt % vanadium oxide loading were prepared using SiO_2 (homemade, pore volume of 0.70 mL g^{-1}, and surface area of 600 m^2 g^{-1}), Nb_2O_5 (CBMM, HY-340, pore volume of 0.18 mL g^{-1}, and surface area of 188 m^2 g^{-1}), and ZrO_2 (Gimex, RC 100, pore volume of 0.23 mL g^{-1}, and surface area of 100 m^2 g^{-1}) as support oxides. The SiO_2 support was prepared via the sol−gel method according to a slightly altered literature recipe;[28] HNO_3 was used instead of HCl. The catalysts were prepared via incipient wetness impregnation using a NH_4VO_3 (Merck, p.a.) solution with oxalic acid (Brocacef, 99.25% pure). The catalysts were dried at room temperature for 1 night, and at 393 K for 1 night and calcined at 773 K for 3 h. All catalysts under investigation, including the 1 wt % alumina-supported vanadium oxide catalyst from our previous paper,[27] are listed in Table 1, together with some physicochemical data and the catalyst code that will be used throughout the paper. The amount of VO_x/nm^2 on the catalysts is compared to the theoretical monolayer for monomers (2.3 VO_x/nm^2) and for polymers (7.5 VO_x/nm^2) as described by Khodakov et al.[7]

2.2. Spectroscopic Characterization. *2.2.1. UV−Vis−NIR DRS and ESR and Raman Spectroscopies.* UV−vis−NIR DRS, ESR, and Raman measurements were performed on dehydrated catalyst samples treated under identical environmental conditions. For this purpose, a special cell with a quartz window for Raman and UV−vis−NIR and a side tube for ESR was used; details on this equipment can be found elsewhere.[29] Dehydration was performed in a stream of O_2 (40 mL min^{-1}) at 723 K for 3 h. Raman spectra (exposure time 50 s, 50 accumulations) were collected at room temperature with a Kaiser RXN spectrometer equipped with a 532 nm diode laser. A 5.5 in. noncontact objective was used for beam focusing and collection of scattered radiation. UV−vis−NIR DRS measurements were carried out at room temperature on a Cary 500 UV−vis−NIR spectrometer from Varian in the range 200−2200 nm. The diffuse reflectance accessory was set to collect diffuse reflected light only. The scans were made with an averaging time of 0.1 s, data interval of 1 nm, and a scan rate of 600 nm/min. Baseline correction was performed using a Halon white standard. ESR measurements were performed with an X-band ESP 300 E spectrometer from Bruker, equipped with a TE_{104} cavity, at 120 K.

2.2.2. EXAFS, IR, and Raman Spectroscopies. X-ray absorption fine structure experiments were carried out at beamline E4 in HASYLAB (Hamburg, Germany) using a Si(111) monochromator. The measurements were performed in fluorescence mode, using an ion chamber filled with 400 mbar N_2 to determine I_0. The detector was a seven-element solid state (SiLi) detector. The monochromator was detuned to 80% of the maximum intensity at the V K-edge (5465 eV) to minimize the presence of higher harmonics. The measurements were carried out in an in situ cell with Kapton windows. Details on the cell design can be found elsewhere.[30] Data were collected at 77 K after dehydration (623 K for 2 h in 2.5% O_2/He, 100 mL min^{-1}), and two or three scans were averaged.

The EXAFS data analysis was carried out using the XDAP code developed by Vaarkamp et al.[31] The background was subtracted by employing cubic spline routines with a continuously adjustable smooth parameter.[32] This led to the normalized oscillatory part of the XAFS data, for which all the contributions to the spectrum, including the atomic X-ray absorption fine structure (AXAFS), were maximized.[32]

The EXAFS data analysis program XDAP allows one to perform multiple-shell fitting in *R*-space by minimizing the residuals between both the absolute and the imaginary part of the Fourier transforms (FTs) of the data and the fit. *R*-space fitting has important advantages compared to the usually applied fitting in *k*-space and is extensively discussed in a paper by Koningsberger et al.[32] The difference file technique was applied together with phase-corrected FTs to resolve the different contributions in the EXAFS data.[32] The exact fit procedure has been described in previous papers by our group.[27,32] Details on the manufacturing of the V−O, V−V, V−Si, V−Nb, and V−Zr backscattering amplitudes and phase shifts are provided in Appendix 1.

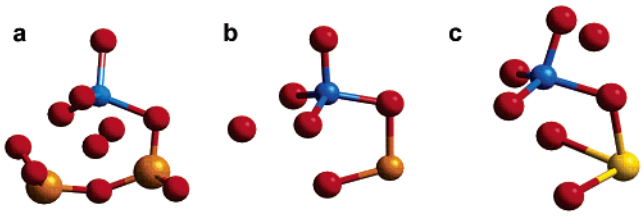

Figure 2. Graphical representation of the structural models for the supported vanadium oxide, obtained with Cerius[2]: (a) all atoms observed with EXAFS for the umbrella model on the (111) plane of β-SiO_2; (b) all atoms observed with EXAFS for the umbrella model on the Nb_2O_5(001) plane; (c) all atoms observed with EXAFS for the umbrella model on the ZrO_2(100) plane.

Additional IR measurements were carried out on self-supported wafers of the catalysts after dehydration at 700 K using a Perkin-Elmer 2000 Fourier transform infrared spectrometer with deuterated triglycine sulfate detector making use of the same in situ cell used for the EXAFS measurements (Kapton windows have been replaced by CaF_2 windows) and mimicking the experimental measuring conditions at 77 K. In a similar fashion, Raman spectra also were measured of these samples.

2.3. Structural Models for Supported Vanadium Oxide Clusters. Structural models for the support surfaces of niobia, silica, and zirconia were constructed using the Cerius[2] molecular modeling software.[33] A VO_4 unit was anchored to the support surface. The obtained structural model was used as an auxiliary to determine the EXAFS input parameters for fitting the higher-coordination shells. For the VO_4 unit anchored onto the SiO_2 surface two structural models were prepared. The crystalline structures for α- and β-quartz were taken from the Cerius[2] database. The surfaces chosen were the (111) surface of β-quartz and the (100) surface of α-quartz, shown in Appendix 2 (Figure A1). The (111) surface is one of the preferentially exposed surfaces for β-SiO_2, and it has a triangle of oxygen atoms present on the surface, which is necessary to accommodate the classical pyramid model of VO_4 with three bonds to the support.[34] Other low index surfaces of β-quartz (e.g., the (001) surface) did not contain such a triangle. The (100) surface of α-quartz, which is preferentially exposed,[35] contains an oxygen triangle as well. This is also illustrated in Appendix 2 (Figure A1). The crystal of Nb_2O_5 was prepared according to the structure determined by Gruehn.[36] The oxygen-terminated (001) surface has been chosen to accommodate the VO_4 cluster. The (100) surface of monoclinic ZrO_2, from the Cerius[2] database, was found to be most suitable to anchor the VO_4 cluster. Both the EXAFS-determined structures and the classical structure with three bonds to the surface were assessed with help of the structural models.

TABLE 3: Interatomic Distances for the Classical Model (with Three Bonds to the Support) for the β-SiO_2(111)-Supported VO_4 Molecule, the α-SiO_2(100)-Supported VO_4 Molecule, the Nb_2O_5(001)-Supported VO_4 Molecule, and the ZrO_2(100)-Supported VO_4 Molecule[a]

model	V=O	V−O	V···$M_{support}$[b]
Classical Model on the (111) Surface of β-SiO_2			
β-SiO_2 (classic)	1.58	1.77	1.73
		2.00	
		2.03	
Classical Model on the (111) Surface of α-SiO_2			
α-SiO_2 (classic)	1.58	1.76	1.39
		1.76	
		1.96	
Classical Model on the (001) Surface of Nb_2O_5			
Nb_2O_5-A (classic)	1.58	2.81	3.34
		2.23	3.21
		2.83	3.64
Nb_2O_5-B (classic)	1.58	1.73	1.30
		1.72	
		1.73	
Classical Model on the (100) Surface of ZrO			
ZrO_2-A (classic)	1.58	1.78	2.17
		1.79	
		1.77	
ZrO_2-B (classic)	1.58	1.75	2.22
		1.85	3.94
		1.82	3.54

[a] On the niobium oxide surface and the zirconia surface two options, A and B, have been explored. [b] M = Si, Nb, or Zr support cation.

For the umbrella model VO_4 unit on all supports, the V=O and the V−O distances were set according to the results obtained from the EXAFS analysis including V=O, V−O, and V···$M_{support}$ (M = Si, Nb, or Zr) distances. Rotation of the molecule around the $M_{support}$−O bond and bending of the V−O−$M_{support}$ bond were the only performed operations to find a suitable configuration of the molecule on top of the surface, where the V···$M_{support}$ distance was used as a structural constraint on all surfaces. An energy minimization was not performed. After rotation of the molecule to a suitable position, the distances from the vanadium atom to the nearest support cations and the nearest support oxygen atoms were determined. The final higher-shell EXAFS fits were determined after several iteration steps with the molecular model obtained from Cerius[2]. Distances to neighboring atoms were determined for the umbrella model and classical on top of β-SiO_2(111), α-SiO_2-(100), Nb_2O_5(001), and ZrO_2(100). The final models, with all atoms fitted with EXAFS, are depicted in Figure 2, and the distances obtained from all the models are listed in Tables 2 and 3.

TABLE 2: Interatomic Distances and Coordination Numbers, Obtained from the Cerius[2] Structural Models, for the Umbrella Model on Several Supports: The β-SiO_2(111)-Supported VO_4 Molecule, the Nb_2O_5(001)-Supported VO_4 Molecule, and the ZrO_2(100)-Supported VO_4 Molecule

	VO_4 supported on the (111) surface of β-SiO_2				VO_4 supported on the (001) surface of Nb_2O_5			VO_4 supported on the (100) surface of ZrO_2		
shell	atom pair	distance (Å)		coordination number	atom pair	distance (Å)	coordination number	atom pair	distance (Å)	coordination number
1	V=O	1.58		1	V=O	1.58	1	V=O	1.58	1
2	V−O	1.77		3	V−O	1.71	3	V−O	1.77	3
3	V···Si	2.6		1	V···O	2.46	1	V···O	2.30	1
4	V···O	2.67	2.68	2	V···O	2.69	1	V···O	2.65	1
5	V···Si	2.95		1	V···Nb	2.81	1	V···Zr	3.15	1
6	V···O	3.2		1				V···O	3.24	1
7	V···O	3.65	3.76	4						
		3.79	3.94							
8	V···O	4.27		1						

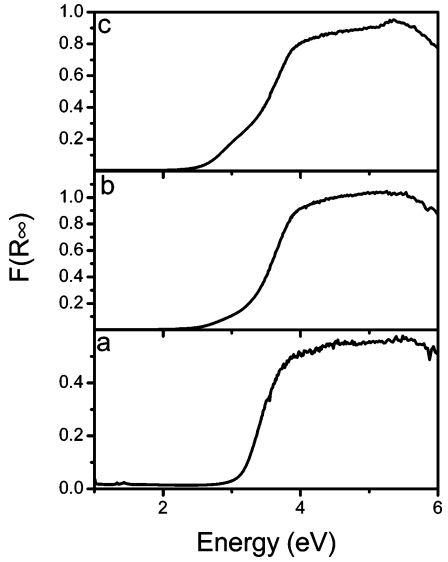

Figure 3. UV−vis−NIR DRS spectra of samples (a) 1V−Si, (b) 1V−Nb, and (c) 1V−Zr measured at room temperature, after dehydration.

3. Results

3.1. Spectroscopic Measurements. Figure 3 shows UV−vis−NIR DRS spectra of the supported vanadium oxide catalysts measured under dehydrated conditions. The DRS spectra are dominated by intense charge transfer (CT) transitions of the $O^{2-} \rightarrow V^{5+}$ (d^0) type. The onset of the CT band (Table 1), determined via the method of Delgass, changes slightly with the support oxide.[37] (The intercept of the straight line at the low-energy rise of a plot of $(F(R\infty)h\nu)^2$ against $h\nu$ was used to determine the edge energy (E_{edge}) for allowed transitions.) It is important to stress that d−d transitions, which are typical for reduced vanadium oxide species, are not observed in any of our samples. This is further confirmed by ESR measurements, which showed no significant amount (<1%) of V^{4+} (d^1).

The Raman spectra of the 1 wt % supported vanadium oxide catalysts are presented in Figure 4A. All spectra show a band in the 1020−1040 cm^{-1} region (Table 1), which has been assigned to the V═O stretch vibration of monomeric species.[16] Bands at 1050 and 800 cm^{-1} are due to the quartz sample container.[38] For 1V−Nb and 1V−Zr the bands below 950 cm^{-1} are due to the support itself, except for one band at 915 and 827 cm^{-1} for 1V−Si and 1V−Zr, respectively, that is associated with vanadium oxide. For 1V−Nb a similar band is probably obscured by support oxide bands.

For dimeric or polymeric species, i.e., containing V−O−V moieties, one would expect to observe V−O−V stretch and bend vibrations. The V−O−V antisymmetric stretch vibration is located between 830 and 630 cm^{-1}.[39−42] The Raman spectra do not contain bands between 830 and 630 cm^{-1} that are associated with the vanadium oxide species, except for 1V−Zr (827 cm^{-1}). The V−O−V symmetric stretch and bend vibrations should be observed at lower frequencies. However, these bands were not observed for any of the catalysts indicating that no dimeric or polymeric vanadium oxide species are present on the support surfaces.

The pre-edge and XANES region for the 1 wt % vanadium oxide catalysts are shown in Figure 4B. According to Wong et al.[43] the height of the pre-edge peak compared to the height of the edge jump allows us to determine the symmetry of the species found on the surface. For a perfect tetrahedron this value is 0.8−1.0. The value observed for the catalysts is between 0.51 and 0.64, indicating that the molecular structure of the vanadium

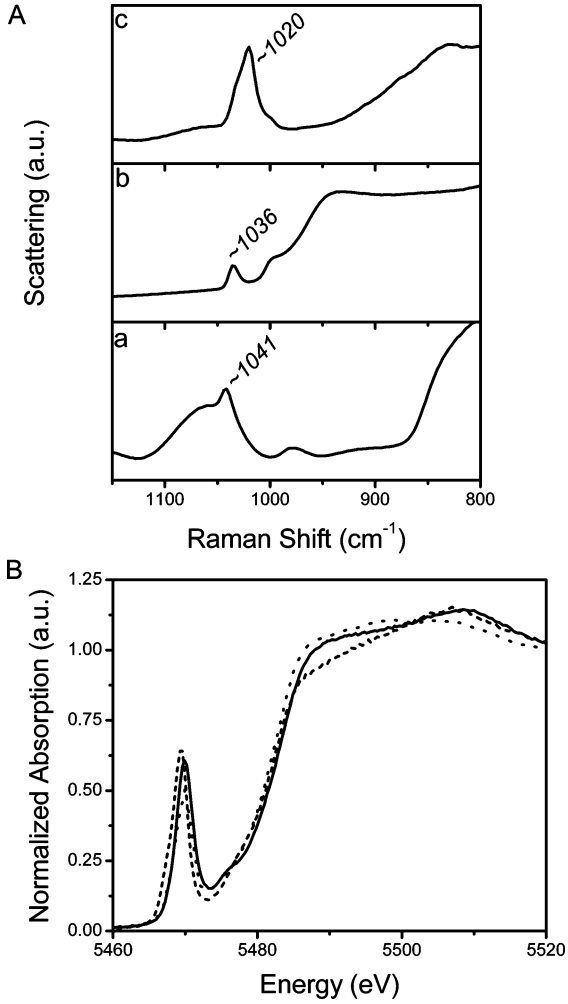

Figure 4. (A) Raman spectra of (a) 1V−Si, (b) 1V−Nb, and (c) 1V−Zr measured under dehydrated conditions at room temperature. (B) Pre-edge and XANES region of the XAFS spectra of samples (a) 1V−Si (—), (b) 1V−Nb (- - -), and (c) 1V−Zr (•••) with clear pre-edge peaks, measured at 77 K after dehydration.

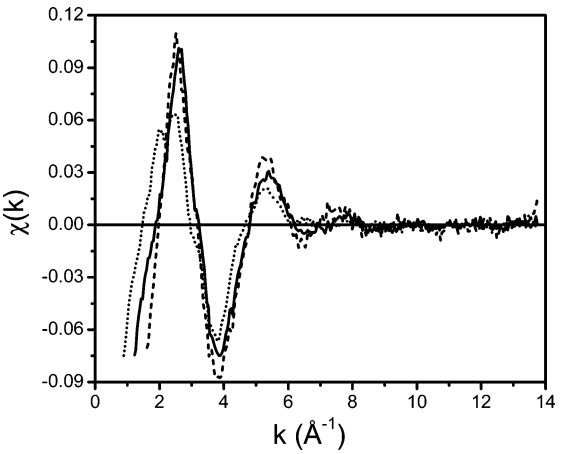

Figure 5. Experimental EXAFS data ($\chi(k)$) of 1V−Nb (—), 1V−Si (- - -), and 1V−Zr (•••) measured at 77 K after dehydration.

oxide species resembles a distorted tetrahedron. This is fully consistent with the results obtained from Raman and in line with the results for an alumina-supported sample.[27] From Figure 5 presented in the article by Wong et al. it can be seen that the difference in energy between the pre-edge peak and the edge is a measure for the oxidation state of vanadium.[43] For all samples a value between 12.62 and 13.62 eV was observed, as listed in

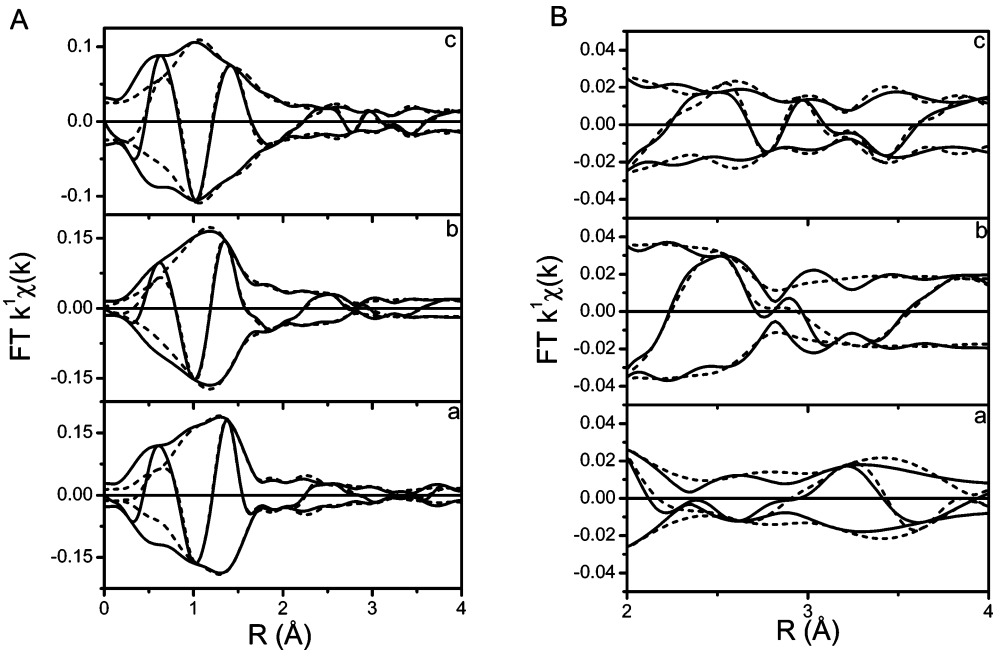

Figure 6. (A) k^1-Weighted Fourier transform ($\Delta k = 2.5-11$ Å^{-1}, $\Delta R = 0.7-4.0$ Å) of the experimental $\chi(k)$ (—) and the final fit (- - -) for (a) 1V−Si, (b) 1V−Nb, and (c) 1V−Zr. (B) Extension of the k^1-weighted Fourier transform in the higher R region ($R = 2-4$ Å) to show differences in higher shells due to support atoms: (a) 1V−Si, (b) 1V−Nb, and (c) 1V−Zr.

Table 1. Literature values for tetrahedral V(V) species vary between 12.4 eV for NH_4VO_3 and 13.5 eV for vanadinite ($Pb_5(VO_4)_3Cl$).[43] For a square pyramidal V(V) (V_2O_5) the $E_{edge} - E_{pre\text{-}edge}$ value is 9.5 eV.[43] This strongly points toward the presence of a tetrahedral coordinated V^{5+} species, which is in agreement with our previous data on an alumina-supported catalyst.[27] The results of Raman and XANES data so far point to the predominant presence of an isolated VO_4 species with vanadium in its 5+ oxidation state in the low loaded supported vanadium oxide catalysts.

3.2. EXAFS Data Analysis and Structural Models. The EXAFS spectra ($\chi(k)$) obtained after background subtraction and normalization are presented in Figure 5. Although the overall shapes of the EXAFS spectra functions are similar, the nodes of the EXAFS oscillations at low values of k do not coincide. This is a strong indication that variations may exist in the molecular structure of the interfacial geometry and the vanadium oxide clusters deposited on the different support materials. The signal-to-noise ratio is ∼34 for 1V−Si, ∼68 for 1V−Nb, and ∼50 for 1V−Zr, with the amplitude determined between $k = 2.5$ and 4 Å^{-1} and the noise level between $k = 11$ and 13 Å^{-1}. The FTs of the raw data (solid lines) are shown in Figure 6A. All data contain a large peak in the 1.5−2 Å region, which can be ascribed to the VO_4 cluster. On the lower R side (<0.7 Å) of this peak the AXAFS contribution is visible. The features at higher values of R are due to higher-shell contributions from the support and are plotted on an expanded scale in Figure 6B. Differences in shape and position are observed in the FTs for values of $R > 2$ Å, implying that the structure of the interface between the vanadium cluster and the support oxide is different.

To illustrate the EXAFS data analysis procedure the analysis of the data for the silica-supported catalyst will be presented in detail before the results of the final fits for the other supported vanadium oxide catalysts are given.

3.2.1. Structure of the VO_4 Cluster: Two-Shell Fit for 1V−Si. From the Raman spectrum we know that one short V═O bond (1.58 Å) is present, as derived from the observed vibration frequency (1020−1040 cm^{-1}).[39] From the XANES data we deduced that the coordination number around vanadium is four. The information obtained from the XANES and Raman spectra, i.e., one V═O bond at 1.58 Å and three V−O bonds, is used as input parameters for the EXAFS fit. This means that only five free parameters are needed to fit the first two coordination shells.

The fit results for the two-shell fit are listed in Table 4, and the FTs of the raw data and the two-shell fit are presented in Figure 7a. A reasonable fit in R-space ($\Delta R = 0.7-2$ Å) could be obtained for $0.7 < R < 1.7$ Å with a distorted tetrahedral VO_4 unit, one oxygen atom at a small distance of 1.58 Å (V═O bond) and three oxygen atoms at a larger distance of 1.75 Å (V−O bond). The distances are similar to the distances observed in the literature and will be further discussed below.[44,45] It can be seen that for values of $R > 1.7$ Å the amplitude of the fit is larger than the amplitude of the FT of the raw data, indicating that a two-shell fit does not describe the experimental data for $R > 1.7$ Å. This is further illustrated in Figure 7b by plotting the FT of the difference file of the raw data minus the first (V═O) and second (V−O) shells, which represent the VO_4 monomer. This residue does not consist only of the FT of the AXAFS function; it obviously contains higher-shell contributions that were not included in the fit. A peak around 1.8 Å is clearly visible in the residue. In summary, at least one extra coordination shell should be introduced in the EXAFS fit.

3.2.2. Structure of the Interface: Three-Shell Fit for 1V−Si. On the basis of the idea that the vanadium oxide cluster is connected to the surface of the support with only one V−O−Si bond, as has been shown previously by the Scott group (V−O−Si) and our group (V−O−Al), only one silicon atom was incorporated in the third shell.[22,24,25,27,44] The fit parameters obtained for the three-shell fits are presented in Table 4. As one can see from Figure 7c the fit describes the data much better for $0.7 < R < 2.5$. Moreover, the FT of the difference file (Raw − $O_{(1)}$ − $O_{(2)}$, solid line) and the fit of the third shell (dotted line, Figure 7d) show that the peak around 1.8 Å can be described by one V···Si coordination at 2.47 Å. The amplitude of the FT of the fit decreases upon the addition of a silicon

TABLE 4: Structural Parameters from *R*-Space Fits of the Experimental EXAFS ($\Delta k = 2.5-11$; $\Delta R = 0.7-4.0$) for Sample 1V−Si[a]

fit	scattering pair	CN[b]	R[c] (Å)	$\Delta\sigma^2$ [d]	ΔE_0[e]	N_{free}[f]	N_{fit}[g]	variances % imaginary part	variances % absolute part
two shell	V═$O_{(1)}$	1[h]	1.58[h]	−0.00350	4.39	9	5	1.9	1.6
	V−$O_{(2)}$	3[h]	1.75	−0.00293	3.91				
three shell	V═$O_{(1)}$	1[h]	1.58[h]	−0.00350	8.53	11.7	8	0.98	1.1
	V−$O_{(2)}$	3[h]	1.76	−0.00228	2.02				
	V···$Si_{(3)}$	1[h]	2.47	0.0102	15.08				
seven shell, β-SiO_2	V═$O_{(1)}$	1[h]	1.58[h]	−0.00350	6.43	19.8	20	1.2	1.1
	V−$O_{(2)}$	3[h]	1.77	−0.00265	4.59				
	V···$Si_{(3)}$	1[h]	2.61	0.0133	7.17				
	V···$O_{(4)}$	2[h]	2.73	0.0180	1.63				
	V···$Si_{(5)}$	1[h]	2.95	0.0160	−7.37				
	V···$O_{(6)}$	1[h]	3.25	0.00400	10.76				
	V···$O_{(7)}$	4[h]	3.67	0.0124	−5.64				

[a] A two-shell fit with one V═O and three V−O, a three-shell fit with one V═O, three V−O, and one V···Si, and a seven-shell fit based on the β-SiO_2(111)-supported umbrella model. [b] CN is the coordination number. [c] R is the distance. [d] $\Delta\sigma^2$ is the Debye−Waller factor, i.e. disorder. [e] E_0 is the inner potential. [f] N_{free} is the maximum number of free parameters according to the Nyquist theorem. [g] N_{fit} is the number of parameters used in the fit. [h] These parameters are fixed during the fit.

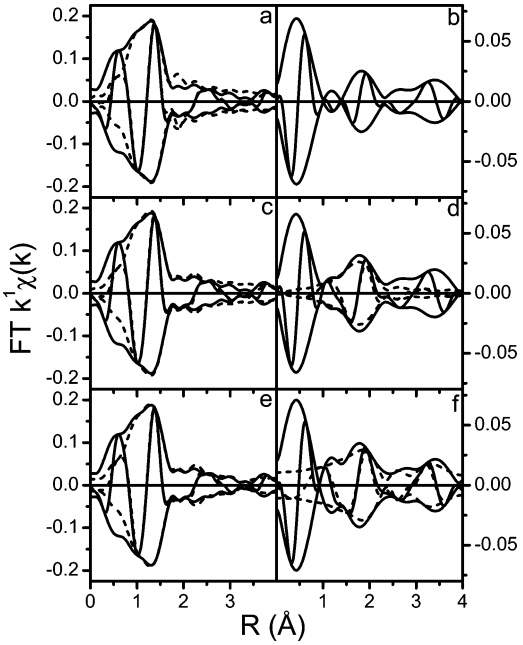

Figure 7. (a) k^1-Weighted Fourier transform ($\Delta k = 2.5-11$ Å^{-1}) of the experimental $\chi(k)$ (—) for 1V−Si and the calculated two-shell fit (- - -) in R-space ($\Delta R = 0.7-2.0$ Å). (b) k^1-Weighted Fourier transform of the residue (Raw − two-shell fit), $\Delta k = 2.5-8$ Å^{-1}, containing the AXAFS at a low R value and higher-shell contributions. This residue indicates that higher shells are needed to complete the fit. (c) k^1-Weighted Fourier transform ($\Delta k = 2.5-11$ Å^{-1}) of the experimental $\chi(k)$ (—) for 1V−Si and the calculated three-shell fit (- - -) in R-space ($\Delta R = 0.7-2.5$ Å). (d) k^1-Weighted Fourier transform of the difference file (Raw − $O_{(1)}$ − $O_{(2)}$), $\Delta k = 2.5-8$ Å^{-1} (—), containing the AXAFS at a low R value and higher-shell contributions, and the difference file for the third shell (- - -). The residue indicates that more than three shells are needed to complete the fit. (e) k^1-Weighted Fourier transform ($\Delta k = 2.5-11$ Å^{-1}) of the experimental $\chi(k)$ (—) for 1V−Si and the calculated seven-shell fit (- - -) in R-space ($\Delta R = 0.7-4.0$ Å) obtained with help of the umbrella model on top of the β-SiO_2(111) plane. (f) k^1-Weighted Fourier transform of the difference file (Raw − $O_{(1)}$ − $O_{(2)}$), $\Delta k = 2.5-8$ Å^{-1}, containing the AXAFS at a low R value and nonseparable higher-shell contributions, and the difference file for the higher shells (- - -), $Si_{(3)} + O_{(4)} + Si_{(5)} + O_{(6)} + O_{(7)}$. The difference file shows that the higher-shell contributions are nicely fit with the seven-shell model.

atom in the third shell, because the first and second shells are out of phase with the third shell.

We have tried to substitute the silicon atom in the fit with a vanadium atom to exclude the presence of dimeric and polymeric species on the support surface. The fit resulted in a very short V···V distance of 2.26 Å, with slightly higher variances. As will be discussed below, a V···V distance of 2.26 Å is too small to account for a dimeric or polymeric species.

3.2.3. Structure of the Interface: Seven-Shell Fit for 1V−Si. As can be seen in Figure 7d, the residue obtained after the three-shell fit still contains various contributions at $R > 2$ Å. Since the number of free parameters is not infinite, we decided to include higher-coordination shells based upon a structural model obtained with Cerius[2]. From this structural model we determined reasonable coordination numbers and possible interatomic distances for the support contributions.

Two structural models were explored to describe the higher-coordination shells of 1V−Si: VO_4 on the (111) surface of β-SiO_2 and VO_4 on the (100) surface of α-SiO_2. The VO_4 unit was positioned on the surface in such a way that only one silicon neighbor is found in the third shell, using the V−$Si_{(3)}$ distance of ∼2.6 Å as a structural constraint. The observed distance in the model turned out to be very close to the distances as obtained with EXAFS (Table 4). The resulting fits and EXAFS parameters for the interfacial structure with β-SiO_2 are listed in Table 4, and the total fit is shown in Figure 7e. The results for the α-SiO_2 fit are presented in the Appendix (Table A3).

A structural model satisfying the conditions outlined above is shown in Figure 2. According to the Cerius[2] model three more V−O shells and one additional V−Si shell should be observed in the EXAFS analysis, in total seven shells. The distances to all neighboring atoms up to ∼4.3 Å are listed in Table 2. The coordination parameters from the Cerius[2] model were used to optimize the analysis of the higher-coordination shells. In Table 4 the resulting EXAFS coordination parameters are given for all seven coordination shells. The interfacial structure based upon the EXAFS coordination parameters is shown in Figure 2a. The FT of the EXAFS fit based upon the iteration with the Cerius[2] model describes the EXAFS data adequately over the whole R-range of $0.7 < R < 5$ Å (Figure 7e). In Figure 7f the FT of the difference file (Raw − $O_{(1)}$ − $O_{(2)}$) and the FT of the EXAFS function representing the fit of the higher-coordination shells ($Si_{(3)} + O_{(4)} + Si_{(5)} + O_{(6)} + O_{(7)}$) are shown. Figure 7f illustrates that the higher shells can be described by shells 3−7. A comparison of the fit of the two-shell fit (Figure 7a) with the total fit (Figure 7e) clearly shows that the total fit also describes

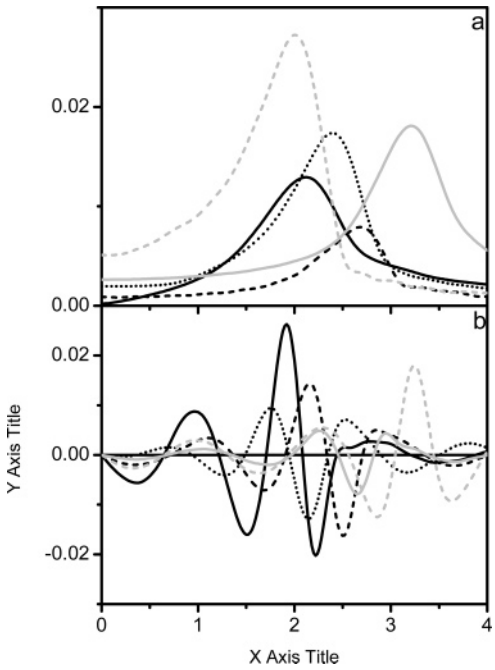

Figure 8. (a) Magnitude of the Fourier transform for the separate shells: $Si_{(3)}$ (—), $O_{(4)}$ (- - -), $Si_{(5)}$ (•••), $O_{(6)}$ (gray solid line), and $O_{(7)}$ (gray dashed line). (b) Imaginary part of the Fourier transform for the separate shells: $Si_{(3)}$ (—), $O_{(4)}$ (- - -), $Si_{(5)}$ (•••), $O_{(6)}$ (gray solid line), and $O_{(7)}$ (gray dashed line). The higher shells do not have the same phase. This means that these contributions will partly cancel out in the total EXAFS fit.

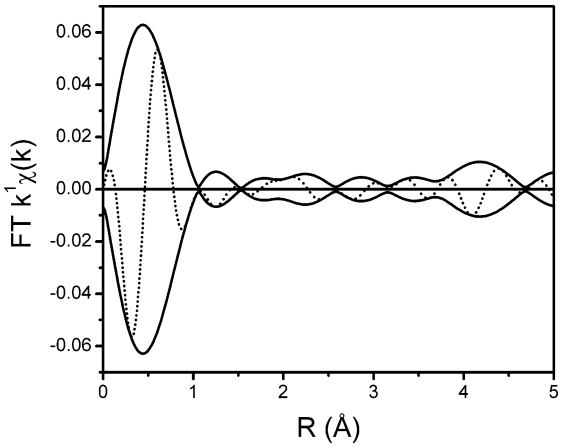

Figure 9. Residue (Raw − total fit), $\Delta k = 2.5-8$ Å^{-1}, for the seven-shell fit from EXAFS of 1V−Si for the model on β-SiO_2, containing the AXAFS and nonseparable higher-shell contributions. The residue indicates the absence of a nonfitted contribution for the umbrella model on top of the (111) plane of β-SiO_2 for $0.7 < R < \sim 4$ Å.

the raw data much better than the two-shell fit in the *R*-range $0.7 < R < 2$ Å.

Figure 8a gives the magnitude of the FTs of each individual coordination shell, showing the peak position of each higher-shell contribution. Figure 8b shows the imaginary parts of the FTs. Clearly, some of the different contributions are in antiphase. This means that interference effects are present and that some of the contributions partially cancel out in the total EXAFS fit. The use of the difference file technique unravels the interference effect.

The FT of the residue (raw data − total seven-shell fit) in Figure 9 shows the AXAFS contribution peaking around 0.5 Å. Moreover, in the *R*-range $0.7 < R < 4$ Å no other higher-shell contributions are visible in the FT of the residue. This

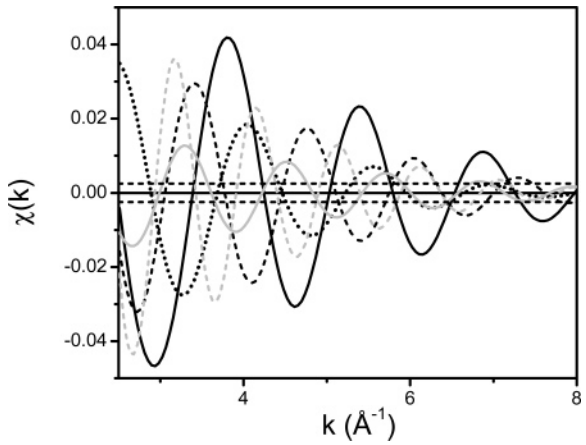

Figure 10. k^0-Weighted χ-function of the separate higher shells obtained from the β-SiO_2 model, $Si_{(3)}$ (—), $O_{(4)}$ (- - -), $Si_{(5)}$ (•••), $O_{(6)}$ (gray solid line), and $O_{(7)}$ (gray dashed line), together with the noise level.

demonstrates that the higher shells are adequately fitted, since no peaks are present in the residue in the range $0.7 < R < 4$. At ~4.2 Å a small contribution is still visible in the residue. Adding an eighth shell to fit this contribution would lead to a better fit; however, our data range was not sufficient to make a fit with eight shells statistically valid.

Variances for the imaginary and absolute part are 1.5 and 1.3, respectively, which shows that the fit is reasonably good. The statistical significance of the higher shells originating from the support can be evaluated from Figure 10, showing the individual EXAFS functions of the higher shells together with the maximum peak-to-peak noise level of ±0.0025. All higher-shell contributions are above the noise level at low values of *k*.

3.2.4. Total Fits for 1V−Nb and 1V−Z. A similar procedure was applied to fit the EXAFS data of 1V−Nb and 1V−Zr. The results of the final fits for 1V−Nb and 1V−Zr are presented in Table 5. The fits are presented in Figure 6A, showing a good agreement between the FT of the data and the FT of the final fit. For both supports only one support cation was observed at an acceptable distance, indicating that the vanadium oxide is anchored to the support with one $V-O-M_{support}$ bond on all supports that were investigated. The structures obtained from the EXAFS fits in combination with the Cerius[2] model for 1V−Nb and 1V−Zr are presented in Figures 2b and 2c.

Table 6 gives an overview of the distances from vanadium to the double-bonded oxygen (V═O), the single-bonded oxygen (V−O), and the support cation for all catalysts under investigation. Data on 1V−Al from our previous paper have been included for comparison.[27] It is clear that the V−O and $V\cdots M_{support}$ distances are influenced by the support oxide. Here all three V−O distances are taken to be equal; however, it has been possible to split the second shell into a shell containing the $V-O_b-M_{support}$ contribution and a shell that contains the two other V−O contributions.[46]

4. Discussion

4.1. Structure of the VO_4 Cluster. There is no dispute in the literature that at low loading the vanadium oxide cluster is present as a 4-fold-coordinated monomer for, e.g., Al_2O_3, SiO_2, TiO_2, and ZrO_2.[47−51] The data presented in this paper lead to the same conclusion for SiO_2, Nb_2O_5, and ZrO_2 supports. Raman, UV−vis−NIR, ESR, and XANES indicate that a monomeric VO_4 species with vanadium in the 5+ oxidation state is present on these support oxides. Raman spectroscopy

TABLE 5: Structural Parameters from *R*-Space Fits of the Experimental EXAFS ($\Delta k = 2.5-11$; $\Delta R = 0.7-3.5$ for 1V−Nb and $\Delta R = 0.7-4.0$ for 1V−Zr) for Samples 1V−Nb and 1V−Zr Based on the Cerius² Models for the Supported Umbrella Model[a]

fit	scattering pair	CN[a]	R[b] (Å)	$\Delta\sigma^2$ [c]	ΔE_0[d]	N_{free}[e]	N_{fit}[f]	variances % imaginary part	variances % absolute part
1V−Nb	V═$O_{(1)}$	1[g]	1.58[g]	0.00137	10.39	17.1	14	0.84	0.68
	V−$O_{(2)}$	2[g]	1.72	0.00331	3.76				
	V···$O_{(3)}$	1[g]	2.43	0.00400	−10.71				
	V···$O_{(4)}$	1[g]	2.64	0.00600	0.88				
	V···$Nb_{(5)}$	1[g]	2.79	0.0153	−6.08				
1V−Zr	V═$O_{(1)}$	1[g]	1.58*	−0.00232	10.00	19.8	17	1.3	1.0
	V−$O_{(2)}$	3[g]	1.77	0.00918	6.07				
	V···$O_{(3)}$	1[g]	2.38	0.0115	−0.49				
	V···$O_{(4)}$	1[g]	2.64	0.0106	7.54				
	V···$Zr_{(5)}$	1[g]	3.15	0.00714	11.51				
	V···$O_{(6)}$	1[g]	3.25	0.00900	0.61				

[a] CN is the coordination number. [b] R is the distance. [c] $\Delta\sigma^2$ is the Debye−Waller factor, i.e. disorder. [d] E_0 is the inner potential. [e] N_{free} is the maximum number of free parameters according to the Nyquist theorem. [f] N_{fit} is the number of parameters used in the fit. [g] These parameters are fixed during the fit.

TABLE 6: Comparison of Bond Distances for All Catalysts, 1V−Al, 1V−Nb, 1V−Si, and 1V−Zr, Including Comparison to Literature Data on SiO_2-Supported $VOCl_3$

atom pair	1V−Al distance (Å)	1V−Nb distance (Å)	1V−Si distance (Å)	distance (Å)	1V−Zr distance (Å)
V═O	1.58	1.58	1.58	1.57	1.58
V−O	1.72	1.72	1.77	1.78	1.77
V−Cl				2.16	
V···$M_{support}$[a]	3.09	2.79	2.61	3.13	3.20
	Keller et al.[27]	this work	this work	Deguns et al.[44]	this work

[a] M = Al, Si, Nb, or Zr support cation.

showed a band between 1020 and 1040 cm^{-1}, which is assigned to a V═O stretch vibration in a monomeric VO_4 species.[16] The V═O (1.58 Å) and V−O (1.72−1.77 Å) distances observed with EXAFS for the VO_4 clusters on SiO_2, Nb_2O_5, and ZrO_2 are similar to the distances observed with EXAFS by Rulkens et al. for the reference compound $OV[OSi(O^tBu)_3]_3$, which has a V═O bond distance of 1.596 Å and three V−O bond distances of 1.770 Å [45] and for $SiOVOCl_2$ which has a V═O distance of 1.57 Å and a V−O distance of 1.78 Å according to Deguns et al.[44]

4.2. Determining the Interfacial Geometry for VO_4 on SiO_2, Nb_2O_5, and ZrO_2. In our previous paper we have determined with EXAFS spectroscopy the interfacial geometry for an alumina-supported vanadium oxide cluster.[27] It was found that the VO_4 cluster is attached to the support with only one V−O_b−Al bond. In the following section the interfacial geometry is discussed for SiO_2-, Nb_2O_5-, and ZrO_2-supported catalysts.

4.2.1. Significance of Higher Shells in the EXAFS Data Analysis and the Use of Cerius² Structural Models. The three-shell fit for 1V−Si (Table 4 and Figure 7a) demonstrates that the third shell consists of only one Si atom, which could be fit within the limit of the number of free parameters. This third shell, containing only one silicon scatterer nearest to the vanadium absorber atom, has been fit reliably without the use of structural models. The presence of a silicon atom in the 3rd shell has already been shown in the literature.[24,25,27,44] An iterative process, using structural models made with the help of Cerius² and the results of the EXAFS data analysis, has led to further insights in the interfacial geometry between VO_4 and the SiO_2 surface. In both the structural models of the silica surface (α-SiO_2 and β-SiO_2) the third shell distance is the same, i.e., 2.61 Å.

Neither the surface of amorphous SiO_2 nor the surfaces of Nb_2O_5 and ZrO_2 are well defined. For silica, the surface will most probably consist of a mixture of structures, similar to quartz surfaces with a tetrahedral coordination of the silicon atoms. The use of structural model surfaces obtained from α- and β-quartz gives an indication of the position of atoms and coordination numbers in higher-coordination shells. The statistical significance of the higher shells originating from the β-SiO_2 support can be evaluated from Figure 10, showing the individual EXAFS functions of the higher shells together with the maximum peak-to-peak noise level of ±0.0025. All higher-shell contributions are above the noise level at low values of k. Variances for the imaginary and absolute part of 1.5 and 1.3, respectively, show that the seven-shell fit of 1V−Si is acceptable.

4.2.2. Quality of the EXAFS Data Analysis: The Number of Free Parameters. When the tetrahedral configuration and the V═O distance are taken as independent inputs for the EXAFS fit, five parameters are required to fit the first two coordination shells (V═$O_{(1)}$ and V−$O_{(2)}$) for all catalysts. Furthermore, the coordination numbers for the higher shells are based upon the Cerius² model. For the seven-shell fit of 1V−Si this means that 20 free parameters ((7 shells × 4 parameters/shell) − 8 fixed input parameters) are required for the total fit (Table 4). According to the Nyquist theorem[52] 19.8 parameters are allowed in the seven-shell 1V−Si EXAFS fit, using $\Delta k = 8.5$ $Å^{-1}$ and $\Delta R = 3.3$ Å. A contribution to the total EXAFS spectrum at $R \approx 3.7$ Å for VO_4/β-SiO_2 and $R \approx 4.1$ Å for VO_4/α-SiO_2 justifies the large R-range used for the fit, considering the large peak width of the seventh shell. This shows that the maximum number of free parameters allowed is not exceeded for this EXAFS fitting process using the VO_4 coordination geometry, the V═O distance, and the coordination numbers from Cerius² model as input parameters.

Neither the 1V−Nb fit nor the 1V−Zr fit exceed the maximum number of free parameters. The 1V−Zr has the same fit range ($\Delta k = 2.5-11$ $Å^{-1}$, $\Delta R = 0.7-4$ Å) as 1V−Si and a maximum of six shells in the total fit. This means that 19.8 free parameters are available, while only 17 are needed when the first shell distance and all coordination numbers are taken as fixed parameters. For the five-shell fit of the 1V−Nb catalyst 17 free parameters are needed when the V═O distance and the distorted tetrahedral coordination are taken as independent parameters, whereas 17.15 are available according to the Nyquist theorem ($\Delta k = 2.5-11$ $Å^{-1}$, $\Delta R = 0.7-3.5$ Å).

4.2.3. V···$M_{support}$ Distances from the EXAFS Analysis Compared to Reference Compounds. The V···Si distance observed for our 1V−Si sample (2.61 Å) is shorter than the V···Si distance reported for $SiOVOCl_2$ (V···Si = 3.13 Å, on the basis of EXAFS). XRD measurements on the reference compounds $VO(OSiPh_3)_3$ and $VOCl(O_2Si^tBu_2)]_3$ showed V··· Si distances of 3.3 and 3.13 Å, respectively.[44,53,54] The different substituents around vanadium in the compounds discussed above, compared to our catalyst, can explain the shorter V···Si distance (0.5−0.7 Å). The substituents of the reference compounds are all larger than a single oxygen atom. One can imagine that it is not possible for the vanadium to get close to the silicon atom due to steric hindrance. For the other supports reference crystalline compounds show that the shortest V··· $M_{support}$ distance is 2.91 Å for $NbVO_5$, ∼3.68 Å for ZrV_2O_7, and ∼3.33 Å for $AlVO_4$.[55−59] For all catalysts under investigation the V···$M_{support}$ distance is shorter than those for the reference compounds. In the case of $AlVO_4$ the Al−O bond distances are much larger than that in the γ-Al_2O_3 used for our model, explaining the larger Al···V distance in the reference compound. For 1V−Nb the Nb−O bond was much longer in the $NbVO_5$ (∼2.3 Å) crystal than that in the Nb_2O_5 support (1.89 Å) as well. For 1V−Zr, however, the Zr−O distance in the model was similar to the distance in ZrV_2O_7. In that case the longer V···Zr distance can partly be explained by a longer V−O distance in ZrV_2O_7 (2.06 Å), compared to the EXAFS results.

4.2.4. Support Cation versus Vanadium Scatterer in the Higher Shells. Although polymeric species are not expected on a silica support according to the literature,[16,60] one could argue whether the third shell in the 1V−Si fit is due to a support cation or a neighboring V scatterer. A neighboring V scatterer is expected to be present, when dimeric, polymeric, or crystalline vanadium oxide species are present on the catalyst surface or in the case that monomeric species are placed very close together at the surface. If two monomers were close together, then the distance between two "neighboring" vanadium atoms would be 6.6 Å for the classical model with three support bonds.[61] This distance is so large that it cannot be observed in our EXAFS data.

In a recent paper by our group we have shown with an extensive analysis of the EXAFS data that on a low loaded alumina-supported vanadium oxide catalyst no V−V scatterer pair is present.[27] When the Si scatterer was replaced by a V scatterer in the three-shell fit a very short distance of 2.26 Å was observed. In dimeric and polymeric species the V···V distance is much larger as is shown by the following literature results. The V···V distance in a polymeric vanadium oxide species is around 3.8 Å, according to Centi.[61] For magnesium divanadate ($Mg_2V_2O_7$), where vanadium is present as a dimer and has a 4-fold oxygen coordination, the V···V distance is 3.42 Å.[62] For ammonium monovanadate (NH_4VO_3), where vanadium is organized in chains, the V···V distance is 3.43 Å,[63] and in vanadium pentoxide (V_2O_5), with pentacoordinated vanadium, the smallest V···V distance is 3.08 Å.[64] The results show that the low loaded SiO_2-supported catalyst does not contain a V···V scatterer pair, which is in total agreement with the Raman data presented above.

4.3. Plausible Models for the Interfacial Structure of VO_4 Clusters on Oxidic Supports. *4.3.1. Evidence for the Classical Model.* Combined NMR and Raman data on TiO_2-supported vanadium oxide led Eckert and Wachs[14] to conclude that a compound of the $Q^{(3)}$-type is present, i.e., $(Ti-O-)_3V{=}O$, although their NMR data only suggested that a species with more than 2-fold symmetry was present. Furthermore, they mentioned that there is no suitable reference compound available to check their suggestion for such a molecular structure. Wachs and co-workers came to the same conclusion for a silica-supported vanadium oxide catalyst.[65] In that case they compared the chemical shifts of their supported vanadium oxide catalysts with two reference compounds ($[Ph_3SiO]_3VO$ and $[(c\text{-}C_6H_{11})_7(Si_7O_{12})VO]_2$). The chemical shifts of the catalyst and the reference compounds match each other, indicating that the vanadium has a 4-fold coordination environment, C_{3v} symmetry, and three V−O−Si bonds.

TABLE 7: Chemical Shift in ^{51}V NMR as a Function of the Number of Chlorine Atoms Attached to Vanadium

	$\delta(^{51}V)$ (ppm)			
	R = Me[76,77]	R = Et[77]	R = ^{i}Pr[77]	R = ^{i}Bu[77]
$VOCl_3$	0	0	0	0
$VOCl_2OR$	−290	−300	−309	−288
$VOCl(OR)_2$		−414	−506	−478
$VO(OR)_3$	−458[a]	−443	−630	−538

[a] Value obtained for sample in tetrahydrofuran.

It is generally known that the chemical shift in NMR is determined by the atoms surrounding the vanadium atom. The first coordination shell will have a profound influence on the value of the chemical shift; however, the second and higher-coordination shells will influence the chemical shift as well. Therefore one can expect that the chemical shift changes with the number of Si atoms around the vanadium atom, as suggested by Wachs and co-workers.[65] Indeed, Lapina et al. have studied the chemical shift for vanadium compounds with varying silicon coordination environments. These authors have shown that the chemical shift for $(SiO)VOCl_2$, with one bond to the support, is much lower (δ_{iso} = −295 ppm) than those for the silica-supported vanadium oxide catalyst (δ_{iso} = −710 ppm) and reference compounds (δ_{iso} = −736 ppm and δ_{iso} = −714 ppm, respectively) reported by Wachs and co-workers.[65,66] However, as is illustrated in Table 7, it has to be mentioned that the chemical shift of $(SiO)VOCl_2$ seems to be influenced profoundly by the number of chlorine ligands and less by the number of silicon ligands. In other words, the influence of the number of silicon neighbors on the chemical shift is not entirely clear. However, severe treatment may have led to some structural changes, enabling the three bonds to the surface.

Went et al.[20] observe a very short V═O bond in their Raman spectra, which resembles the V═O in $VOCl_3$. They conclude that a species with three V−O-support bonds is present on the SiO_2 surface, since $VOCl_3$ has C_{3v} symmetry. Went et al. even suggest four bonds (bond order <1) to the support for a titania-supported vanadium oxide catalyst, even though they realize that the number of V−O−$M_{support}$ bonds cannot be determined with Raman spectroscopy.[67] Anpo et al.[21] mention that the amount of $VOCl_3$ deposited via chemical vapor deposition (CVD) on the SiO_2 surface can be monitored with UV (charge transition of $O^{2-} \rightarrow V^{5+}$) and IR (OH vibration) spectroscopies. The formation of HCl during the reaction indicates that vanadium is anchored to the surface via V−O−Si bonds. Unfortunately, the authors did not link the amount of HCl formed during reaction and calcination nor the amount of OH groups disappearing to the amount of vanadium present and thus did not prove unambiguously that the number of V−O− $M_{support}$ bonds is three.

4.3.2. Comments on the Classical Model and Alternative Models. Various researchers, however, oppose the idea of three bonds to the surface.[22,24−27,68] Both Rice et al. and Keränen et

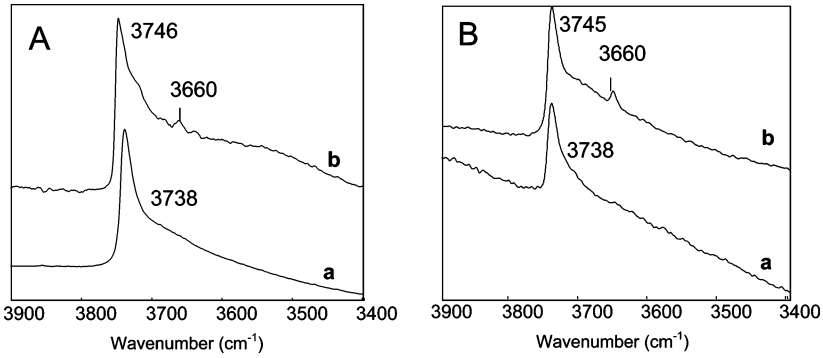

Figure 11. (A) IR and (B) Raman spectra of the OH region of 1V−Si recorded in the in situ EXAFS cell under a flow of He/O_2: (a) dehydrated at 700 K and (b) after cooling to 77 K.

al. have shown that the amount of HCl and propanol released per vanadium atom upon anchoring of a vanadium precursor to the silica support is significantly lower than three.[24−26] Their experiments indicate that the vanadium oxide unit is attached to the support with one or two bonds. Inumaru et al. even claim that it is impossible to reach the state with three bonds to the support due to steric hindrance.[68] Recently, Gijzeman et al. proposed a model with one $V-O-M_{support}$ bond to explain the temperature dependence of the V═O Raman stretch vibration frequency of 1 wt % vanadium oxide catalysts supported on silica and niobia.[22] Density functional theory calculations illustrated that the energy of formation was significantly lower for the umbrella model than that for the classical model.[69] A vanadium oxide species with only one bond to the surface has been reported for $SiOVOCl_2$ based on EXAFS analysis.[24,25,44] Furthermore, a similar molecular structure has been reported for supported rhenium oxide catalysts.[70,71]

In our previous study we have examined the structure of a 1 wt % alumina-supported vanadium oxide catalyst. The molecular structure of the VO_4 cluster (one V═O bond of 1.58 Å and three V−O bonds of 1.72 Å) was determined with EXAFS spectroscopy. Moreover, the EXAFS analysis allowed us to establish the position of the vanadium atom relative to the alumina support O anions and Al cations, resulting in a proposal for the interfacial geometry, including only one $V-O_b-Al$ bond and several other support contributions to the EXAFS spectrum.[27]

Unfortunately, EXAFS does not give detailed information on the exact state of the other two V−O single bonds. We can neither detect a possible bond between the two oxygen atoms from the V−O single bonds as suggested by Gijzeman et al. in the peroxo containing umbrella model,[22] nor is it possible to observe the possible presence of hydrogen atoms (V−OH), as already discussed in our paper on alumina-supported vanadium oxide catalysts.[22,27] To evaluate the possible presence of V−OH bands, IR and Raman spectroscopies have been applied in a separate set of experiments on identical catalyst wafers and measured in the same EXAFS in situ measurement cell, but of course equipped with different spectral windows. The catalyst samples were first measured just after dehydration at 700 K and later on after cooling to 77 K, the temperature at which the EXAFS spectra described in this work and our previous paper[27] have been measured. The results for the 1V−Si catalyst are given in Figure 11. Both IR and Raman reveal one single and intense band at 3738 cm^{-1}, which is commonly assigned to a Si−OH vibration. After the sample was cooled to 77 K an additional sharp band was detected centered at 3660 cm^{-1}, which can be assigned to a V−OH vibration. In other words, a very plausible surface species under the experimental conditions applied has the following molecular structure: $O═V(OH)_2-O_b-M_{support}$. It is important to indicate that the Raman spectrum in the region between 1100 and 800 cm^{-1} after cooling to 77 K remained almost unaltered, the only change being the shift of the V═O vibration from 1046 to 1035 cm^{-1}. Thus, small traces of water present in the EXAFS measurement cell may be responsible for the partial rehydration of the catalyst material leading to the formation of one or two V−OH groups, although the overall molecular structure of the supported vanadium oxide species with one V═O bond and one $V-O_b-M_{support}$ bond remained unaltered.

Finally, several structural models where vanadium is attached with three bonds to the surface of the support were investigated with Cerius^2. Possible $V\cdots M_{support}$ distances were determined with Cerius^2, with the V−O distances according to the EXAFS results for the $V═O_{(1)}$ and $V-O_{(2)}$ shells (Table 3). It was impossible to adjust all three $V-O-M_{support}$ bonds in the Cerius^2 model to the distance obtained with EXAFS. In most cases the $V\cdots M_{support}$ distance determined with the Cerius^2 models was too short compared to the EXAFS results. Only for ZrO_2-B (classic) two $V\cdots M_{support}$ distances were longer than the distance obtained from EXAFS, and for the Nb_2O_5-A (classic) all three $V\cdots M_{support}$ distances were longer. One could argue that for the ZrO_2-B model the average distance is 3.23 Å, which is close to the distance obtained with EXAFS. However, the difference between the three values is so large that these should be easily separated with EXAFS.

These considerations make it clear that the classical model could not be accommodated on the support surfaces, except major surface restructuring is taking place. It has to be emphasized that the EXAFS measurements are carried out at liquid nitrogen temperatures, which may have resulted in the adsorption of traces of water. However, at high temperatures surface reconstruction may take place, enabling the formation of a VO_4 cluster with three bonds to the support. Possible mechanisms of reconstructions and the influence of the vanadium thereupon are, to our best knowledge, unknown. Therefore, we chose to use the original atom positions obtained from the crystalline oxide structures produced with Cerius^2. Moreover, the presence of a Si scatterer at 2.61 Å was unambiguously established with EXAFS alone. This excludes a necessary surface reconstruction at least for 1V−Si.

Without a surface reconstruction formation of a surface species with two bonds to the silica surface is impossible, taking into consideration the short V−O distances of 1.77 Å observed with EXAFS. The V−O distances from the two V−O−Si bonds obtained from Cerius^2 were ∼2.12 Å, which is too long, and the V···Si distances were about 2.45 Å, which is too short. However, additional experimental proof will be required to discard the molecular structure with two bonds to the supporting oxide as a viable vanadium oxide surface species. Therefore,

TABLE A1: Crystallographic Data and the Input Parameters for FEFF 8 Used To Create the Theoretical Reference Files for the V−O, the V−$M_{support}$, and the V−V Scatterer Pair

atom pair	reference compound	ref	N	R (Å)	σ^2	V_r (eV)	V_i (eV)	S_0^2
V−O	Na_3VO_4	75	4	1.696	0.004	−2.2	1	0.84
V−Nb			1	3.00	0	0	1	0.80
V−Si			1	3.00	0	0	1	0.80
V−Zr			1	3.00	0	0	1	0.80
V−V			1	3.00	0	0	1	0.80

all Cerius[2] models should be envisaged as plausible structures to accommodate the umbrella VO_4 unit and enabling to fit the higher shells of the EXAFS data. By no means, they can be seen as exclusive solutions simply because no detailed structural information on amorphous silica, niobia, or zirconia is currently available. However, the EXAFS data analysis results together with the Cerius[2] models for all supports suggest an interfacial structure in which the vanadium oxide cluster is attached to the surface with only one V−O−$M_{support}$ bond, showing that the umbrella model is viable for all supports under investigation and under the measurement conditions applied.

5. Concluding Remarks

Raman, XANES, and EXAFS showed that after dehydration 1 wt % vanadium oxide supported on Al_2O_3, SiO_2, Nb_2O_5, and ZrO_2 is tetrahedral coordinated. One V=O bond of 1.58 Å and three V−O bonds with distances ranging from 1.72 to 1.77 Å have been detected. It was demonstrated that higher shells have to be included in the EXAFS data analysis to fit the data properly and to elucidate the interfacial geometry of vanadium supported on Al_2O_3, SiO_2, Nb_2O_5, and ZrO_2. For the 1V−Si sample it has been unequivocally demonstrated that only one Si scatterer is present in the third shell at 2.61 Å, showing that the VO_4 cluster is anchored to the surface of the SiO_2 support via one V−O_b−Si bond. The EXAFS results combined with structural modeling using Cerius[2] software lead to one unique V−O_b−$M_{support}$ interaction for all investigated supports, where the exact V−O_b and the V···$M_{support}$ distances depend on the type of oxidic support. The data presented in this paper show that the umbrella model proposed for supported monomeric vanadium oxide catalysts is viable for the low loaded supported vanadium oxide catalysts studied in this paper. Additional IR and Raman spectra measured under almost identical conditions as those of the EXAFS measurements reveal the presence of V−OH groups, suggesting that a plausible surface species on the supports under investigation is of the type O=V$(OH)_2$−O_b−$M_{support}$. Further experimental and theoretical studies will verify if this molecular structure is indeed representing the state of supported vanadium oxide catalysts (under reaction conditions) and may explain metal oxide support effects observed in

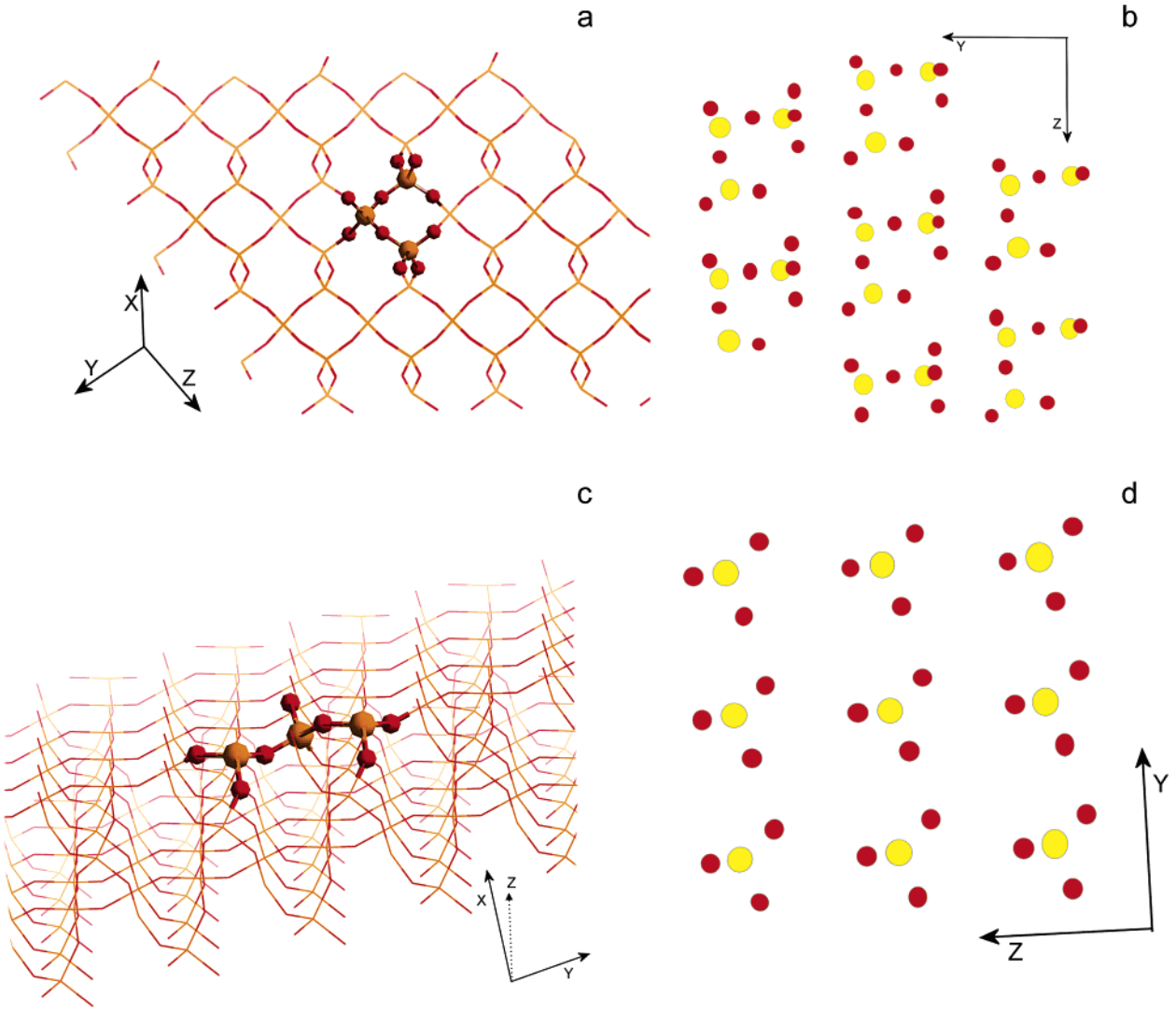

Figure A1. Graphical representation of the structural models obtained with Cerius[2] for the SiO_2 support: (a) the β-SiO_2(111) plane, (b) top view of the β-SiO_2(111) plane, (c) the α-SiO_2(100) plane, and (d) top view of the α-SiO_2(100) plane.

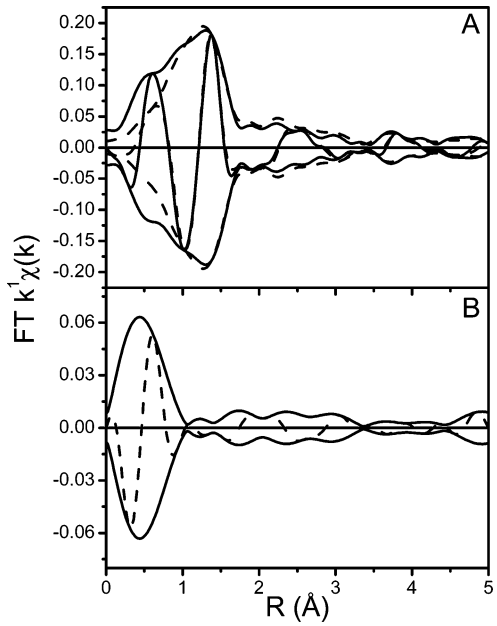

Figure A2. (a) k^1-Weighted Fourier transform ($\Delta k = 2.5-11$ Å^{-1}) of the experimental $\chi(k)$ (—) for 1V−Si, the calculated fit (- - -) in R-space ($\Delta R = 0.7-5.0$ Å) obtained with help of the umbrella model on top of the α-SiO_2(100) plane. (b) k^1-Weighted Fourier transform of the residue (Raw − total fit) $\Delta k = 2.5-8$ Å^{-1}, containing the AXAFS at a low R value and nonseparable higher-shell contributions. The residue indicates the absence of a nonfitted contribution for the umbrella model on top of the (100) plane of α-SiO_2 for $0.7 < R < \sim 4$ Å.

TABLE A2: Interatomic Distances and Coordination Numbers for the α-SiO_2(100)-Supported VO_4 Molecule, Obtained from the Model Produced with Cerius[2]

VO_4 supported on the (100) surface of α-SiO_2				
atom pair		distance (Å)		coordination number
V═O		1.58		1
V−O		1.77		3
V···Si		2.6		1
V···O		2.84		1
V···O		3.28		1
V···Si	3.93	4.14		2
V···O	4.07	4.55	4.66	5
		4.72	4.78	

selective oxidation and oxidative dehydrogenation reactions. In any case, the described experiments also reveal that the applied measurement conditions clearly affect the molecular structure of supported vanadium oxides making detailed comparisons between the many spectroscopic results available in the literature far from trivial.

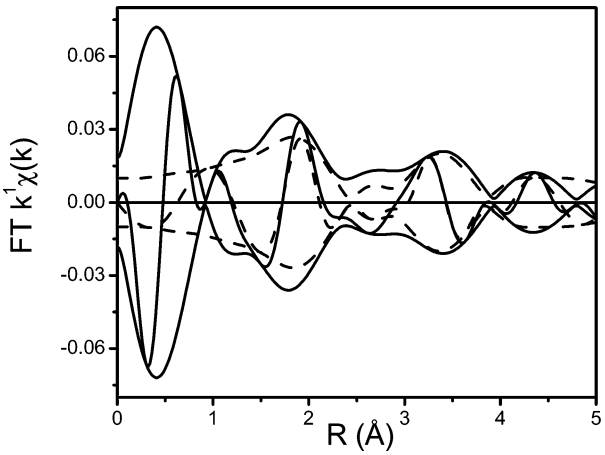

Figure A3. k^1-Weighted Fourier transform of the difference file (Raw − $O_{(1)}$ − $O_{(2)}$) $\Delta k = 2.5-8$ Å^{-1}, containing the AXAFS at a low R value and nonseparable higher-shell contributions, and the difference file for the higher shells (- - -), $Si_{(3)} + O_{(4)} + O_{(5)} + Si_{(6)} + O_{(7)}$, obtained from the α-$SiO_2$ model.

Acknowledgment. The EXAFS work at the HASYLAB beam station was supported by the IHP contract HPRI-CI-2001-00140 of the European Commission. B.M.W acknowledges financial support from the NRSCC, NWO/CW-Van der Leeuw, NWO/CW-VICI, and a EU-COST D15 program.

Appendices

Appendix 1. Reference Compounds and FEFF 8 Calculations. Data for the V−O and V···$M_{support}$ phase shift and backscattering amplitude were obtained from calculations with the FEFF 8 code.[72,73] The scattering potentials are calculated by overlapping free atom electron densities within the well-known muffin-tin approximation. In this study, the Hedin−Lundqvist (HL) potential[74] was used to calculate the phase shift and backscattering amplitude. The theoretical V−O reference was calibrated with the experimental Na_3VO_4 EXAFS data using an R-space fit. The input parameters of the FEFF8 code were adjusted until the experimental reference was fitted with $\Delta\sigma^2 = 0$ and $\Delta E_0 = 0$, and the distance ($R = 1.696$ Å) and the coordination number (CN = 4) agree with the crystallographic data.[75] This resulted in a theoretical reference with a larger k-range than that of the experimental data. The reference spectra were measured at room temperature; the sample was measured at liquid nitrogen temperature. This means that, besides a difference in structural disorder, a temperature effect has to be included in the difference in the Debye−Waller factor ($\Delta\sigma^2$) between the sample and the reference as obtained in the EXAFS data analysis. For the V···$M_{support}$ and V···V scatterer pair the

TABLE A3: Structural Parameters from All R-Space Fits of the Experimental EXAFS ($\Delta k = 2.5-11$; $\Delta R = 0.7-4.0$) for Sample 1V−Si[a]

								variances	
fit	scattering pair	CN[b]	R[c] (Å)	$\Delta\sigma^2$ [d]	ΔE_0[e]	N_{free}[f]	N_{fit}[g]	imaginary part	absolute part
seven shell, α-SiO_2	V═$O_{(1)}$	1[h]	1.58[h]	−0.00274	10.76	19.8	20	1.5	1.3
	V−$O_{(2)}$	3[h]	1.77	−0.00156	0.07				
	V···$Si_{(3)}$	1[h]	2.61	0.0119	−0.16				
	V···$O_{(4)}$	1[h]	2.96	0.00200	8.38				
	V···$O_{(5)}$	1[h]	3.16	0.00200	8.38				
	V···$Si_{(6)}$	2[h]	3.98	0.00768	−0.16				
	V···$O_{(7)}$	5[h]	4.38	0.0350	−13.18				

[a] A seven-shell fit based on the α-SiO_2(100)-supported umbrella model. [b] CN is the coordination number. [c] R is the distance. [d] $\Delta\sigma^2$ is the Debye−Waller factor, i.e. disorder. [e] E_0 is the inner potential. [f] N_{free} is the maximum number of free parameters according to the Nyquist theorem. [g] N_{fit} is the number of parameters used in the fit. [h] These parameters are fixed during the fit.

distance between the vanadium (absorber) atom and the scatterer atom (Nb, Si, Zr, or V) was set to 3.00 Å. The $\chi(k)$-functions were calculated for $k = 0$ Å^{-1} to $k = 20$ Å^{-1}. Suitable experimental reference compounds were not available to us for calibration purposes. The input parameters used to calculate the theoretical references are listed in Table A1.

Appendix 2. Structural Models of SiO_2 Surfaces. Figure A1 shows the graphical representations of two structural models obtained with Cerius^2 for the SiO_2 support surface.

Appendix 3. Fit for 1V−Si Based on the Cerius^2 Model for the VO_4 Molecule Supported on the (100) Surface of α-SiO_2. The same procedure as described in detail for the VO_4 supported on the (111) surface of β-SiO_2 was followed for a model on α-quartz (100). The final fit and residue are shown in Figure A2, and the fit parameters are included in Table A3. This fit is of the same quality as that for β-quartz-(111)-supported VO_4. The variances for the imaginary (1.5) and absolute (1.3) part are in the same range. However, when the FT of the fit for $(Si_{(3)} + O_{(4)} + O_{(5)} + Si_{(6)} + O_{(7)})$ is compared to the FT of Raw $- O_{(1)} - O_{(2)}$, Figure A3, one can see that the fit of the higher shells for the α-quartz model is deviating from the data more than the fit for the β-quartz.

References and Notes

(1) Deo, G.; Wachs, I. E. *J. Catal.* **1994**, *146*, 323.
(2) Olthof, B.; Khodakov, A.; Bell, A. T.; Iglesia, E. *J. Phys. Chem. B* **2000**, *104*, 1516.
(3) Bañares, M. A. *Catal. Today* **1999**, *51*, 319.
(4) Burcham, L. J.; Wachs, I. E. *Catal. Today* **1999**, *49*, 467.
(5) Bañares, M. A.; Martínez-Huerta, M. V.; Gao, X.; Fierro, J. L. G.; Wachs, I. E. *Catal. Today* **2000**, *61*, 295.
(6) Gao, X.; Wachs, I. E. *Top. Catal.* **2002**, *18*, 243.
(7) Khodakov, A.; Olthof, B.; Bell, A. T.; Iglesia, E. *J. Catal.* **1999**, *181*, 205.
(8) Koningsberger, D. C.; de Graaf, J.; Mojet, B. L.; Ramaker, D. E.; Miller, J. T. *Appl. Catal., A* **2000**, *191*, 205.
(9) Ramaker, D. E.; Dorssen, G. E. van; Mojet, B. L.; Koningsberger, D. C. *Top. Catal.* **2000**, *10*, 157.
(10) van der Eerden, A. M. J.; Visser, T.; Nijhuis, T. A.; Ikeda, Y.; Lepage, M.; Koningsberger, D. C.; Weckhuysen, B. M. *J. Am. Chem. Soc.* **2005**, *127*, 3272.
(11) Wachs, I. E. *Catal. Today* **1996**, *27*, 437.
(12) Takenaka, S.; Tanaka, T.; Yamazaki, T.; Funabiki, T.; Yoshida, S. *J. Phys. Chem. B* **1997**, *101*, 9035.
(13) Oyama, S. T.; Went, G. T.; Lewis, K. B.; Bell, A. T.; Somorjai, G. A. *J. Phys. Chem.* **1989**, *93*, 6786.
(14) Eckert, H.; Wachs, I. E. *J. Phys. Chem.* **1989**, *93*, 6796.
(15) Le Coustumer, L. R.; Taouk, B.; Le Meur, M.; Payen, E.; Guelton, M.; Grimblot, J. *J. Phys. Chem.* **1988**, *92*, 1230.
(16) Gao, X.; Bare, S. R.; Weckhuysen, B. M.; Wachs, I. E. *J. Phys. Chem. B* **1998**, *102*, 10842.
(17) Weckhuysen, B. M.; Jehng, J.-M.; Wachs, I. E. *J. Phys. Chem. B* **2000**, *104*, 7382.
(18) Busca, G. *J. Raman Spectrosc.* **2002**, *33*, 348.
(19) Eckert, H.; Deo, G.; Wachs, I. E.; Hirt, A. M. *Colloids Surf.* **1990**, *45*, 347.
(20) Went, G. T.; Oyama, S. T.; Bell, A. T. *J. Phys. Chem.* **1990**, *94*, 4240.
(21) Anpo, M.; Sunamoto, M.; Che, M. *J. Phys. Chem.* **1989**, *93*, 1187.
(22) Gijzeman, O. L. J.; Lingen, J. N. J. v.; Lenthe, J. H. V.; Tinnemans, S. J.; Keller, D. E.; Weckhuysen, B. M. *Chem. Phys. Lett.* **2004**, *397*, 277.
(23) Bond, G. C.; Perez Zurita, J.; Flamerz, S.; Gellings, P. J.; Bosch, H.; Ommen, J. G. v.; Kip, B. J. *Appl. Catal.* **1986**, *22*, 361.
(24) Rice, G. L.; Scott, S. L. *J. Mol. Catal. A: Chem.* **1997**, *125*, 73.
(25) Rice, G. L.; Scott, S. L. *Langmuir* **1997**, *13*, 1545.
(26) Keränen, J.; Guimon, C.; Iiskola, E.; Auroux, A.; Niinisto, L. *J. Phys. Chem. B* **2003**, *107*, 10773.
(27) Keller, D. E.; de Groot, F. M. F.; Koningsberger, D. C.; Weckhuysen, B. M. *J. Phys. Chem. B* **2005**, *109*, 10223.
(28) Weckhuysen, B. M.; de Ridder, L. M.; Schoonheydt, R. A. *J. Phys. Chem.* **1993**, *97*, 4756.
(29) Weckhuysen, B. M.; Schoonheydt, R. A. *Catal. Today* **1999**, *49*, 441.
(30) Kampers, F. W. H.; Maas, T. M. J.; Grondelle, J. v.; Brinkgreve, P.; Koningsberger, D. C. *Rev. Sci. Instrum.* **1989**, *60*, 2635.
(31) Vaarkamp, M., Linders, J. C., Koningsberger, D. C. *Physica B* **1995**, *208/209*, 159.
(32) Koningsberger, D. C.; Mojet, B. L.; Dorssen, G. E. v.; Ramaker, D. E. *Top. Catal.* **2000**, *10*, 143.
(33) *Cerius^2*, version 3.5; Molecular Simulations, Inc.: San Diego, CA, 1997.
(34) Ferreira, M. L.; Volpe, M. *J. Mol. Catal. A: Chem.* **2002**, *184*, 349.
(35) de Leeuw, N. H.; Higgins, F. M.; Parker, S. C. *J. Phys. Chem. B* **1999**, *103*, 1270.
(36) Gruehn, R. *J. Less-Common Met.* **1966**, *11*, 119.
(37) Delgass, W. N.; Haller, G. L.; Kellerman, R.; Lunsford, J. H. *Spectroscopy in Heterogeneous Catalysts*; Academic Press: New York, 1979.
(38) Zheng, X.; Fu, W.; Albin, S.; Wise, K. L.; Javey, A.; Cooper, J. B. *Appl. Spectrosc.* **2001**, *55*, 382.
(39) Hardcastle, F. D.; Wachs, I. E. *J. Phys. Chem.* **1991**, *95*, 5031.
(40) Frost, R. L.; Erickson, K. L.; Weier, M. L.; Carmody, O. *Spectrochim. Acta. Part A* **2005**, *61*, 829.
(41) Gao, X.; Jehng, J.-M.; Wachs, I. E. *J. Catal.* **2002**, *209*, 43.
(42) Baltes, M.; Cassiers, K.; Van der Voort, P.; Weckhuysen, B. M.; Schoonheydt, R. A.; Vansant, E. F. *J. Catal.* **2001**, *197*, 160.
(43) Wong, J.; Lytle, F. W.; Messmer, R. P.; Maylotte, D. H. *Phys. Rev. B* **1984**, *30*, 5596.
(44) Deguns, E. W.; Taha, Z.; Meitzner, G. D.; Scott, S. L. *J. Phys. Chem. B* **2005**, *109*, 5005.
(45) Rulkens, R.; Male, J. L.; Terry, K. W.; Olthof, B.; Khodakov, A.; Bell, A. T.; Iglesia, E.; Tilley, T. D. *Chem. Mater.* **1999**, *11*, 2966.
(46) Keller, D. E.; Airaksinen, S. M. K.; Krause, A. O. I.; Weckhuysen, B. M.; Koningsberger, D. C., to be submitted for publication.
(47) Weckhuysen, B. M.; Keller, D. E. *Catal. Today* **2003**, *78*, 25.
(48) Deo, G.; Wachs, I. E.; Haber, J. *Crit. Rev. Surf. Chem.* **1994**, *4*, 141.
(49) Inumaru, K.; Misono, M.; Okuhara, T. *Appl. Catal., A* **1997**, *149*, 133.
(50) Wachs, I. E.; Weckhuysen, B. M. *Appl. Catal., A* **1997**, *157*, 67.
(51) Arena, F.; Frusteri, F.; Parmaliana, A. *Appl. Catal., A* **1999**, *176*, 189.
(52) Stern, E. A. *Phys. Rev. B* **1993**, *48*, 9825.
(53) Goschke, R. A.; Vey, K.; Walter, U.; Goering, E.; Klemm, M.; Horn, S. *Surf. Sci.* **1996**, *348*, 305.
(54) Gosink, H.-J.; Roesky, H. W.; Noltemeyer, M.; Schmidt, H.-G.; Freier-Erdmegger, C.; Sheldriek, G. M. *Chem. Ber.* **1993**, *126*, 279.
(55) Brázdová, V.; Ganduglia-Pirovano, M. V.; Sauer, J. *Phys. Rev. B* **2004**, *69*, 165420.
(56) Amarilla, J. M.; Casal, B.; Ruiz-Hitzky, E. *J. Mater. Chem.* **1996**, *6*, 1005.
(57) Evans, J. S. O.; Hanson, J. C.; Sleight, A. W. *Acta Crystallogr., Sect. B* **1998**, *54*, 705.
(58) Baran, E. J.; Botto, I. M. *Monatsh. Chem.* **1977**, *108*, 311.
(59) Coelho, A. A. *J. Appl. Crystallogr.* **2000**, *33*, 899.
(60) Burcham, L. J.; Deo, G.; Gao, X.; Wachs, I. E. *Top. Catal.* **2000**, *11/12*, 85.
(61) Centi, G. *Appl. Catal., A* **1996**, *14*, 267.
(62) Gopal, R.; Calvo, C. *Acta Crystallogr., Sect. B* **1974**, *30*, 2491.
(63) Evans, H. T., Jr. *Z. Kristallogr.* **1960**, *114*, 257.
(64) Bachmann, H. G.; Ahmed, F. R.; Barnes, W. H. *Z. Kristallogr.* **1961**, *115*, 110.
(65) Das, N.; Eckert, H.; Hu, H.; Wachs, I. E.; Walzer, J. F.; Feher, F. J. *J. Phys. Chem.* **1993**, *97*, 8240.
(66) Lapina, O. B.; Matsko, M. A.; Mikenas, T. B.; Zakharov, V. A.; Paukshtis, E. A.; Khabibulin, D. F.; Sobolev, A. P. *Kinet. Catal.* **2001**, *42*, 553.
(67) Went, G. T.; Leu, L.-J.; Bell, A. T. *J. Catal.* **1992**, *134*, 479.
(68) Inumaru, K.; Okuhara, T.; Misono, M. *J. Phys. Chem.* **1991**, *95*, 4826.
(69) van Lingen, J. N. J.; Gijzeman, O. L. J.; Weckhuysen, B. M.; van Lenthe, J. H. *J. Catal.* **2006**, *239*, 34.
(70) Andreini, A. *J. Mol. Catal.* **1991**, *65*, 359.
(71) Mitra, B.; Gao, X.; Wachs, I. E.; Hirt, M. A.; Deo, G. *Phys. Chem. Chem. Phys.* **2001**, *3*, 1144.
(72) Ankudinov, A. L.; Ravel, B.; Rehr, J. J.; Conradson, S. D. *Phys. Rev. B* **1998**, *58*, 7565.
(73) Mustre de Leon, J.; Rehr, J. J.; Zabinski, S. I.; Albers, R. C. *Phys. Rev. B* **1991**, *44*, 4146.
(74) Hedin, L.; Lundqvist, S. *Solid State Phys.* **1969**, *23*, 1.
(75) Tillmanns, E.; Baur, W. H. *Acta Crystallogr., Sect. B* **1971**, *27*, 2124.
(76) Rehder, D. *Bull. Magn. Reson.* **1982**, *4*, 33.
(77) Rehder, D. *Magn. Reson. Rev.* **1984**, *9*, 125.